J|A|C|S
ARTICLES
Published on Web 02/14/2007

Solvent Effect on Conical Intersections in Excited-State 9H-Adenine: Radiationless Decay Mechanism in Polar Solvent

Shohei Yamazaki and Shigeki Kato*

Contribution from the Department of Chemistry, Graduate School of Science, Kyoto University, Kitashirakawa, Sakyo-ku, Kyoto 606-8502, Japan

Received September 26, 2006; E-mail: shigeki@kuchem.kyoto-u.ac.jp

Abstract: The ground- and excited-state free energy minima and the conical intersections among these states of 9H-adenine in aqueous and acetonitrile solutions are studied theoretically to elucidate the mechanism of radiationless decay. We employ the recently proposed linear-response free energy (LRFE) to locate the energy minima and conical intersections in solution. The LRFE is calculated by using the reference interaction site model self-consistent field method. The geometry optimizations are carried out at the complete active space self-consistent field level, and the dynamic electron correlation energies are estimated by the multireference Møller−Plesset method. We find that the conical intersection between the ^1L_a and ^1L_b states in aqueous solution occurs at a wide area of the free energy surface, indicating a strong vibronic coupling between them. On the other hand, the $^1n\pi^*$ state is largely blue-shifted at planar geometries in solution, which suggests that the nonadiabatic transition to this state is suppressed. The importance of the $^1\pi\sigma^*$ channel is also examined in both the gas phase and solution. Based on the free energy characteristics obtained by the calculations, we intend to explain the experimental observations that the excited state of 9H-adenine decays monoexponentially with shorter lifetimes in polar solvents than that in the gas phase.

1. Introduction

DNA/RNA bases show a high degree of photostability. Recent femtosecond time-resolved spectroscopic experiments have established that they undergo ultrafast internal conversion with the picosecond (ps) or sub-ps time scale after the absorption of UV light.[1] The 9H isomer of adenine (9H-adenine) is one of the prototype molecules to exhibit such ultrafast radiationless decay. In the gas phase, the transient ionization[2−6] and time-resolved photoelectron[7−9] signals indicate that the excited-state lifetime is about 1 ps or more. Recent experiments further observed biexponential decay of the excited state with sub-ps and ps lifetimes.[4−9] For example, the transient ionization signal consisting of the decay components with the lifetimes of 0.1 and 1.1 ps was reported by Canuel et al.[4]

It has been observed that the excited-state lifetime is significantly affected by solvation. Time-resolved fluorescence[10,11] and transient absorption[12] experiments provide the lifetime on the order of 0.1 ps in aqueous solution. Cohen et al.[12] reported the transient absorption spectra with decay times of 0.18 ± 0.03 ps and 0.44 ± 0.07 ps for 9H-adenine in aqueous and acetonitrile solutions, respectively. For the aqueous solution, the fluorescence upconversion spectrum gave a similar decay time of 0.23 ± 0.05 ps.[10] Although the spectra of adenine in solution also show biexponential decay as in the gas phase, only the shorter lifetime component is assigned to 9H-adenine, and the longer one, to the 7H isomer.[10−12] Excitation energy dependence of the fluorescence decay time of 9H-adenine in aqueous solution was also studied, and the observed lifetime varied from 0.34 ± 0.07 ps to 0.67 ± 0.14 ps with decreasing energy.[11] This change is much smaller than that of the gas-phase lifetime which becomes up to several ps at longer excitation wavelengths.[6,7,13]

On theoretical ground, isolated nucleobases have been extensively studied to explain their fast radiationless decays.[5,14−28]

(1) Crespo-Hernández, C. E.; Cohen, B.; Hare, P. M.; Kohler, B. *Chem. Rev.* **2004**, *104*, 1977−2019.
(2) Kang, H.; Lee, K. T.; Jung, B.; Ko, Y. J.; Kim, S. K. *J. Am. Chem. Soc.* **2002**, *124*, 12958−12959.
(3) Kang, H.; Jung, B.; Kim, S. K. *J. Chem. Phys.* **2003**, *118*, 6717−6719.
(4) Canuel, C.; Mons, M.; Piuzzi, F.; Tardivel, B.; Dimicoli, I.; Elhanine, M. *J. Chem. Phys.* **2005**, *122*, 074316.
(5) Ritze, H.-H.; Lippert, H.; Samoylova, E.; Smith, V. R.; Hertel, I. V.; Radloff, W.; Schultz, T. *J. Chem. Phys.* **2005**, *122*, 224320.
(6) Samoylova, E.; Lippert, H.; Ullrich, S.; Hertel, I. V.; Radloff, W.; Schultz, T. *J. Am. Chem. Soc.* **2005**, *127*, 1782−1786.
(7) Ullrich, S.; Schultz, T.; Zgierski, M. Z.; Stolow, A. *J. Am. Chem. Soc.* **2004**, *126*, 2262−2263.
(8) Ullrich, S.; Schultz, T.; Zgierski, M. Z.; Stolow, A. *Phys. Chem. Chem. Phys.* **2004**, *6*, 2796−2801.
(9) Satzger, H.; Townsend, D.; Zgierski, M. Z.; Patchkovskii, S.; Ullrich, S.; Stolow, A. *Proc. Natl. Acad. Sci. U.S.A.* **2006**, *103*, 10196−10201.
(10) Gustavsson, T.; Sharonov, A.; Onidas, D.; Markovitsi, D. *Chem. Phys. Lett.* **2002**, *356*, 49−54.
(11) Pancur, T.; Schwalb, N. K.; Renth, F.; Temps, F. *Chem. Phys.* **2005**, *313*, 199−212.
(12) Cohen, B.; Hare, P. M.; Kohler, B. *J. Am. Chem. Soc.* **2003**, 125, 13594−13601.
(13) Lührs, D. C.; Viallon, J.; Fischer, I. *Phys. Chem. Chem. Phys.* **2001**, *3*, 1827−1831.
(14) Sobolewski, A. L.; Domcke, W.; Dedonder-Lardeux, C.; Jouvet, C. *Phys. Chem. Chem. Phys.* **2002**, *4*, 1093−1100.
(15) Sobolewski, A. L.; Domcke, W. *Eur. Phys. J. D* **2002**, *20*, 369−374.
(16) Marian, C. M. *J. Chem. Phys.* **2005**, *122*, 104314.

Conical intersections (CIs) between different electronic states have been recognized to be an important clue in interpreting their short excited-state lifetimes. For 9H-adenine, several CIs among the excited states and between the ground and excited ones have been located by ab initio calculations,[16−23] and various decay pathways have been proposed, including (i) the ring puckering direct decay channel from the ^1L_a state,[17,22,23] (ii) the decay path through the $^1n\pi^*$ state,[16−19,21−23] and (iii) the pathway via the Rydberg-type $^1\pi\sigma^*$ state leading to the dissociation of an NH bond.[5,14−16,18]

Compared with the research activities for isolated nucleobases, theoretical studies on the radiationless decay processes of solvated ones are still limited.[5,29−31] Particularly, studies on the CIs under solvent environments are virtually nonexistent, to our knowledge, in spite of the fact that the structures of CIs are largely affected by the solvation.[32−34] Recently we proposed a method for locating minimum free energy CI geometries in solution,[34] employing the reference interaction site model self-consistent field (RISM-SCF) method.[35,36] We defined a free energy corresponding to nonequilibrium solvation conditions based on the linear-response theory, referred to as the linear-response free energy (LRFE).[34] With this method, the solute nuclear coordinates and solvation ones are simultaneously optimized to determine CIs as well as energy minima.

In the present paper, we study the free energy profiles of $\pi\pi^*$ (^1L_a and ^1L_b),$^1n\pi^*$, and $^1\pi\sigma^*$ excited states as well as the ground state of 9H-adenine in aqueous and acetonitrile solutions using the LRFE optimization. We focus on the solvent effects on the geometries and energies of these states and the CIs between them. Since the decay dynamics of the excited states in a polar solvent is much different from that in the gas phase, we also perform calculations under isolated conditions to compare with the results in solution. Geometry optimizations are carried out by employing the complete active space (CAS) SCF wave functions, and multireference Møller−Plesset (MRMP) calculations[37,38] are repeated at the optimized geometries to take into account the dynamic electron correlation effect.

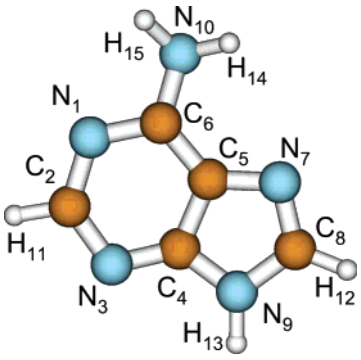

Figure 1. Atom labeling of 9H-adenine.

The purpose of this work is to provide a plausible explanation for the decay time difference of the excited-state 9H-adenine in aqueous solution from the gas phase, based on the free energy characteristics obtained by the calculations.

2. Computational Details

The LRFE at the electronic state I is defined as[34]

$$F^I_{LR}(\mathbf{R},\mathbf{V},\mathbf{U}) = \langle\Psi^I(\mathbf{R},\mathbf{V})|\hat{H}_0 + \hat{\mathbf{Q}}^t\mathbf{V}|\Psi^I(\mathbf{R},\mathbf{V})\rangle + \epsilon^t\mathbf{U} + \frac{1}{2\beta}(\mathbf{V}^t\,\mathbf{U}^t)\,\sigma^{-1}(\mathbf{R})\begin{pmatrix}\mathbf{V}\\ \mathbf{U}\end{pmatrix} \quad (1)$$

where $\mathbf{R}$ is the solute nuclear coordinate and $\mathbf{V}$ and $\mathbf{U}$ are, respectively, the solvent electrostatic and Lennard−Jones (LJ) potentials acting on the solute atomic sites, regarded as the solvation coordinates. Ψ^I is the solute electronic wave function for the state I, $\hat{H}_0$ is the solute electronic Hamiltonian in the gas phase, $\hat{\mathbf{Q}}$ is the operator that generates the partial charge on each atomic site in solute, and ϵ is the vector of solute LJ parameters. The vectors $\mathbf{U}$ and ϵ are defined in ref 34. β is the inverse of k_BT with k_B as the Boltzmann constant and T as the temperature, respectively. In the last term of eq 1, σ is the covariance matrix representing the fluctuations of $\mathbf{V}$ and $\mathbf{U}$, given by

$$\sigma = \begin{pmatrix}\langle\Delta\mathbf{V}\Delta\mathbf{V}^t\rangle & \langle\Delta\mathbf{V}\Delta\mathbf{U}^t\rangle\\ \langle\Delta\mathbf{U}\Delta\mathbf{V}^t\rangle & \langle\Delta\mathbf{U}\Delta\mathbf{U}^t\rangle\end{pmatrix} \quad (2)$$

where $\Delta\mathbf{V}$ and $\Delta\mathbf{U}$ are the deviations of $\mathbf{V}$ and $\mathbf{U}$ from their equilibrium averages, respectively. At the equilibrium solvation, the LRFE in eq 1 becomes the usual linear response free energy,

$$F^I_{LR}(\mathbf{R},\bar{\mathbf{V}}_I,\bar{\mathbf{U}}_I) = \left\langle\Psi^I(\mathbf{R},\bar{\mathbf{V}}_I)\middle|\hat{H}_0 + \frac{1}{2}\hat{\mathbf{Q}}^t\bar{\mathbf{V}}_I\middle|\Psi^I(\mathbf{R},\bar{\mathbf{V}}_I)\right\rangle + \frac{1}{2}\epsilon^t\bar{\mathbf{U}}_I \quad (3)$$

where $\bar{\mathbf{V}}_I$ and $\bar{\mathbf{U}}_I$ are the equilibrium averages of electrostatic and LJ potentials for the state I.

Optimizations of the minimum and CI geometries were carried out in the gas phase and solutions (H_2O and CH_3CN). The solute wave functions were obtained at the state-averaged (SA) CASSCF level. We employed the (9s5p1d/4s1p)/[3s2p1d/2s1p] basis set.[39] For describing the $^1\pi\sigma^*$ state, this basis set was further augmented with the s and p functions with the exponent of 0.028 and 0.025,[39] respectively, on N_9 and the s function with the exponent of 0.02 on H_{13} (see Figure 1 for the atom labeling). All of the geometries were optimized without any symmetry restriction (C_1 symmetry), and some of them were also optimized under C_s symmetry constraint in order to examine the effect of out-of-plane deformation. For the ground and $^1\pi\pi^*$ (^1L_a and ^1L_b) state minima, the active space of CASSCF calculations was constructed by distributing 12 electrons in 10 π orbitals, referred to as CAS(12,-

(17) Perun, S.; Sobolewski, A. L.; Domcke, W. *J. Am. Chem. Soc.* **2005**, *127*, 6257−6265.
(18) Perun, S.; Sobolewski, A. L.; Domcke, W. *Chem. Phys.* **2005**, *313*, 107−112.
(19) Nielsen, S. B.; Sølling, T. I. *ChemPhysChem* **2005**, *6*, 1276−1281.
(20) Matsika, S. *J. Phys. Chem. A* **2005**, *109*, 7538−7545.
(21) Chen, H.; Li, S. *J. Phys. Chem. A* **2005**, *109*, 8443−8446.
(22) Blancafort, L. *J. Am. Chem. Soc.* **2006**, *128*, 210−219.
(23) Serrano-Andrés, L.; Merchán, M.; Borin, A. C. *Chem.−Eur. J.* **2006**, *12*, 6559−6571.
(24) Ismail, N.; Blancafort, L.; Olivucci, M.; Kohler, B.; Robb, M. A. *J. Am. Chem. Soc.* **2002**, *124*, 6818−6819.
(25) Merchán, M.; Serrano-Andrés, L. *J. Am. Chem. Soc.* **2003**, *125*, 8108−8109.
(26) Matsika, S. *J. Phys. Chem. A* **2004**, *108*, 7584−7590.
(27) Zgierski, M. Z.; Patchkovskii, S.; Fujiwara, T.; Lim, E. C. *J. Phys. Chem. A* **2005**, *109*, 9384−9387.
(28) Chen, H.; Li, S. *J. Chem. Phys.* **2006**, *124*, 154315.
(29) Mennucci, B.; Toniolo, A.; Tomasi, J. *J. Phys. Chem. A* **2001**, *105*, 4749−4757.
(30) Gustavsson, T.; Bányász, Á.; Lazzarotto, E.; Markovitsi, D.; Scalmani, G.; Frisch, M. J.; Barone, V.; Improta, R. *J. Am. Chem. Soc.* **2006**, *128*, 607−619.
(31) Gustavsson, T.; Sarkar, N.; Lazzarotto, E.; Markovitsi, D.; Barone, V.; Improta, R. *J. Phys. Chem. B* **2006**, *110*, 12843−12847.
(32) Toniolo, A.; Granucci, G.; Martínez, T. J. *J. Phys. Chem. A* **2003**, *107*, 3822−3830.
(33) Burghardt, I.; Cederbaum, L. S.; Hynes, J. T. *Faraday Discuss.* **2004**, *127*, 395−411.
(34) Yamazaki, S.; Kato, S. *J. Chem. Phys.* **2005**, *123*, 114510.
(35) Ten-no, S.; Hirata, F.; Kato, S. *J. Chem. Phys.* **1994**, *100*, 7443−7453.
(36) Sato, H.; Hirata, F.; Kato, S. *J. Chem. Phys.* **1996**, *105*, 1546−1551.
(37) Hirao, K. *Chem. Phys. Lett.* **1992**, *190*, 374−380.
(38) Nakano, H. *J. Chem. Phys.* **1993**, *99*, 7983−7992.
(39) Dunning, T. H., Jr.; Hay, P. J. In *Methods of Electronic Structure Theory*; Schaefer, H. F., III, Ed.; Plenum: New York, 1977.

10)(10π). For the ^{1}nπ* state minimum, the two lowest π orbitals were replaced by the two lone pair ones at the pyrimidine ring; that is, the active space of CAS(12,10)(8π2n) was employed. For the $^1\pi\sigma$* state, a Rydberg σ orbital was further included in the active space, i.e., CAS(12,11)(10π1σ). The CI optimizations were performed with the CAS(12,10)(8π2n) except for the $^1L_a/^1L_b$ and $^1L_a/^1\pi\sigma$* CIs. State averaging was carried out over two, three, or four singlet states with equal weights, denoted as SA2, SA3, or SA4, respectively, while the state-specific CASSCF method was employed for the optimization of ground-state geometry. These active spaces and state averaging are summarized in the Supporting Information.

The covariance matrix σ was analytically evaluated by the RISM-SA-CASSCF method.[34] The potential parameters for the solvent molecules H_2O and CH_3CN and the LJ parameters for adenine were taken from the literatures.[40−42] For H_2O, the LJ parameters $\sigma = 1.0$ Å and $\epsilon = 0.056$ kcal/mol were added to the H sites. The densities for H_2O and CH_3CN solvents are 0.997 and 0.777 g/cm^3, respectively. The RISM integral equation was solved with the hypernetted-chain (HNC) closure relation at a temperature of 298.15 K.[43] In the solute wave function and covariance matrix calculations, the partial charges on the solute atomic sites were determined by a least-squares fitting procedure to the electrostatic potential around the solute molecule.[35] To avoid the divergence of the partial charges, the restricted electrostatic potential (RESP) scheme was employed.[44]

At the CASSCF optimized geometries, the solute electronic energies were recalculated at the MRMP level.[37,38] For the ground, $^1\pi\pi$*, and ^{1}nπ* states, the active space was constructed by distributing 16 electrons in 12 orbitals (10 π and 2 lone pair orbitals), and the five lowest singlet states were averaged with equal weights, referred to as SA5-CAS(16,12)(10π2n), to obtain the reference SA-CASSCF wave functions. The MRMP energy for the $^1\pi\sigma$* state was calculated based on the SA4-CAS(12,11)(10π1σ) wave functions. The solvated Fock operator was used to construct the zeroth-order Hamiltonian. The intruder state avoidance method with the shift parameter of 0.02 was employed.[45] The covariance matrix was recalculated at the RISM-SA-CASSCF level with these active spaces.

The MRMP energies of two crossing states at the CASSCF optimized CI geometries would be separated due to the difference of dynamic electron correlations between the two states. To locate the CI point at the MRMP level, the solute geometry was corrected with the displacement in the direction of the gradient difference vector. The displacement vector $\Delta\mathbf{x}$ for a CI between the states I and J was estimated by

$$\Delta\mathbf{x} = -\frac{\Delta E^{IJ}}{|\mathbf{g}^{IJ}|^2}\mathbf{g}^{IJ} \tag{4}$$

where ΔE^{IJ} is the energy difference at the MRMP level and $\mathbf{g}^{IJ}$ is the difference of gradient vectors at the CASSCF level. If the gradient difference at the MRMP level is equal to $\mathbf{g}^{IJ}$, the MRMP energy gap at the corrected geometry becomes zero to the first order of $\Delta\mathbf{x}$.

In this work, the CASSCF and MRMP calculations were carried out by the MOLPRO[46] and GAMESS[47] packages, respectively, in which our own RISM-SCF code was implemented.

Table 1. Vertical Excitation Energies in the Gas Phase and Solution (in eV)[a]

state	gas	CH_3CN	H_2O
	$(gs)_{min}$ (C_s)		
^1L_b	4.96 (0.003)	4.94 (0.003)	4.92 (0.003)
^1L_a	4.98 (0.213)	4.96 (0.199)	4.88 (0.215)
^{1}nπ*	4.98 (0.005)	5.03 (0.005)	5.20 (0.004)
$^1\pi\sigma$*[b]	5.39 (0.001)	5.54 (0.000)	5.42 (0.000)
	$(gs)_{min}$ (C_1)		
^1L_b	4.97 (0.003)	4.96 (0.003)	4.96 (0.010)
^1L_a	5.02 (0.198)	5.05 (0.161)	5.13 (0.119)
^{1}nπ*	4.93 (0.006)	4.92 (0.007)	4.97 (0.010)

[a] Oscillator strengths are in parentheses. [b] Estimated by energy difference from the ^1L_a state energy of $(^1L_a)_{min}$.

3. Results and Discussion

3.1. Ground State and Vertical Excitation Energy. We first optimized the geometry of the ground state, labeled as $(gs)_{min}$, at the CASSCF level. The optimized structure is almost planar with the amino group slightly pyramidalized (see Supporting Information). The extent of pyramidalization becomes larger in solution to enhance the solute−solvent interaction by increasing the solute dipole moment in the out-of-plane direction. The dipole moments obtained by the least-square fitting of partial charges in the gas phase, CH_3CN, and H_2O are 2.70, 3.67, and 5.10 D, respectively. The solvation energy, defined as the free energy change from the solute energy in the gas phase, is 0.43 and 0.96 eV in acetonitrile and aqueous solutions, respectively.

In order to estimate the barrier height of the amino group inversion, we obtained the optimized geometry in planar form (C_s symmetry). The MRMP barrier heights were very low, 0.01, 0.03, and 0.09 eV in the gas phase, CH_3CN, and H_2O, respectively. In aqueous solution, the free energy at the nonplanar geometry under the equilibrium solvent potentials corresponding to the planar one was also calculated, resulting in a very flat free energy curve along the inversion coordinate. These results indicate that the inversion of an amino group readily occurs and the probability taking the planar geometry is rather large even in aqueous solution, considering the zero-point vibration and thermal energies.

Table 1 gives the vertical excitation energies at the planar and nonplanar optimized geometries calculated at the MRMP level. The oscillator strengths are also included. In calculating the excited-state energies, we adopted the electrostatic and LJ potentials, **V** and **U**, obtained for the ground state at the optimized geometries. In the gas phase, the lowest two $^1\pi\pi$* (^1L_a and ^1L_b) and one ^{1}nπ* states are very close in energy at both the C_s and C_1 geometries. The same result was also reported in previous studies.[16,21,22] The ^{1}nπ* state is lowest in energy at the C_1 geometry, and the ^1L_b and ^1L_a energies are higher by 0.04 and 0.09 eV, respectively. At the C_s geometry, the ^1L_b becomes the lowest state and the ^1L_a and ^{1}nπ* states are located higher by 0.02 eV. The ^1L_a state has the largest oscillator strength with the ground state among the three excited states, and thus the photoabsorption of 9H-adenine is attributed to the transition to this state. The calculated excitation energy to the ^1L_a state, 4.98 eV, agrees well with the experimental absorption maximum at 252 nm (4.92 eV).[48] Since the basis set and active

(40) Berendsen, H. J. C.; Postma, J. P. M.; van Gunsteren, W. F.; Hermans, J. In *Intermolecular Forces*; Pullman, B., Ed.; Reidel: Dordrecht, 1981; pp 331−342.
(41) Jorgensen, W. L.; Briggs, J. M. *Mol. Phys.* **1988**, *63*, 547−558.
(42) Cornell, W. D.; Cieplak, P.; Bayly, C. I.; Gould, I. R.; Merz, K. M., Jr.; Ferguson, D. M.; Spellmeyer, D. C.; Fox, T.; Caldwell, J. W.; Kollman, P. A. *J. Am. Chem. Soc.* **1995**, *117*, 5179−5197.
(43) Singer, S. J.; Chandler, D. *Mol. Phys.* **1985**, *55*, 621−625.
(44) Bayly, C. I.; Cieplak, P.; Cornell, W. D.; Kollman, P. A. *J. Phys. Chem.* **1993**, *97*, 10269−10280.
(45) Witek, H. A.; Choe, Y.-K.; Finley, J. P.; Hirao, K. *J. Comput. Chem.* **2002**, *23*, 957−965.
(46) Werner, H.-J. et al. *MOLPRO*, version 2002.6; Birmingham, U.K., 2003; see http://www.molpro.net.
(47) Schmidt, M. W.; Baldridge, K. K.; Boatz, J. A.; Elbert, S. T.; Gordon, M. S.; Jensen, J. H.; Koseki, S.; Matsunaga, N.; Nguyen, K. A.; Su, S.; Windus, T. L.; Dupuis, M.; Montgomery, J. A., Jr. *J. Comput. Chem.* **1993**, *14*, 1347−1363.
(48) Clark, L. B.; Peschel, G. G.; Tinoco, I., Jr. *J. Phys. Chem.* **1965**, *69*, 3615−3618.

Table 2. Relative and Vertical Emission Energies of Excited-State Minima in the Gas Phase and Solution (in eV)

		relative energy[a]			emission energy[b]		
structure	symmetry	gas	CH_3CN	H_2O	gas	CH_3CN	H_2O
$(^1L_b)_{min}$	C_s	4.55	4.55	4.55	4.52 (0.004)	4.49 (0.005)	4.41 (0.009)
	C_1	4.58	4.59	4.59	4.56 (0.002)	4.57 (0.001)	4.57 (0.009)
$(^1n\pi^*)_{min}$	C_1	4.25	4.33	4.31	2.90 (0.005)	3.02 (0.003)	2.91 (0.000)
$(^1L_a)_{min}$	C_s	5.09	4.98	4.91	4.69 (0.148)	4.58 (0.142)	4.39 (0.136)

[a] Measured from the ground-state energy of $(gs)_{min}$ (C_1). [b] Oscillator strengths are in parentheses.

space for the $^1\pi\sigma^*$ state are different from those for the other states, we adopted the energy difference from the ^1L_a state to estimate the energy of the $^1\pi\sigma^*$ state. As seen in Table 1, the $^1\pi\sigma^*$ state is located above the ^1L_a one by 0.41 eV and the oscillator strength is considerably small.

In solution, the vertical excitation energy to ^1L_a state is red-shifted at the planar geometry. The calculated shift of 0.10 eV in aqueous solution is comparable to the experimental value, 0.15 eV.[48,49] The $^1n\pi^*$ state, on the other hand, is blue-shifted by 0.05 and 0.22 eV in CH_3CN and H_2O, respectively, at the planar geometry. The magnitude of blue shift becomes smaller at the C_1 geometry because the solute−solvent electrostatic interaction increases in the $^1n\pi^*$ state due to the induced solute dipole moment in the out-of-plane direction. The energy shift of the ^1L_b state by solvation is small. The vertical excitation energies to the $^1\pi\sigma^*$ state are blue-shifted by 0.17 and 0.35 eV in CH_3CN and H_2O, respectively. In contrast to the calculations of Ritze et al.[5] for adenine−H_2O complexes, where the H_2O position is adjusted to the $^1\pi\sigma^*$ state charge distribution, the energy difference from the ^1L_a state increased by the solvation in the present case because the solvent potentials are in equilibrium to the ground state charge distributions, which do not stabilize the $^1\pi\sigma^*$ state.

3.2. Excited States and Vertical Emission Energy. We obtained the CASSCF optimized geometries for three excited states, $(^1L_b)_{min}$, $(^1n\pi^*)_{min}$, and $(^1L_a)_{min}$. The MRMP energies at the three minima measured from the ground-state energy of $(gs)_{min}$are summarized in Table 2, and their coordinates are given in the Supporting Information. Although the CASSCF energy at the C_1 optimized geometry of ^1L_b state is lower by 0.03 eV than that at C_s symmetry, the planar geometry becomes lower in energy than the nonplanar one due to the difference of dynamic electron correlation energy between the two geometries. The same is true in both H_2O and CH_3CN solvents as seen in Table 2. Thus, it is considered that the equilibrium geometry of ^1L_b state is of the planar form. For ^1L_a state, we were able to locate the minimum energy geometries with C_s symmetry. In the case of C_1 geometry, the optimizations failed due to the root flipping between ^1L_a and ^1L_b states in the SA-CASSCF calculations. We carried out the normal-mode analysis at the optimized geometry of ^1L_a state in the gas phase and obtained one normal coordinate with the imaginary frequency of $240i$ cm^{-1}, which is mainly composed of the pyramidalization of C_2 atom. Therefore, the C_s minimum energy geometry corresponds to the saddle point of the potential energy surface, that is, the ^1L_a state energy decreases by the out-of-plane deformation. Actually, Blancafort[22] and Serrano-Andrés et al.[23] reported that the ^1L_a state optimization in C_1 geometry led to the CI between the ground and ^1L_a states.

Since the geometrical characteristics of excited states in the gas phase are fully discussed previously,[16,17,19,21−23] we summarize the solvation effects on the excited-state geometries here. The bond lengths of ^1L_b and $^1n\pi^*$ states are not affected by the solvation; the changes of distances are within 0.02 Å even in aqueous solution. On the other hand, in the planar ^1L_a geometry, the N_3C_4 bond length increases by 0.04 Å and the C_4N_9 decreases by 0.03 Å in H_2O from the gas-phase values. For $(^1n\pi^*)_{min}$, the out-of-plane deformation of C_2 atom is large in the gas phase, while it is largely suppressed in aqueous solution.

As seen in Table 2, the $^1n\pi^*$ state is the lowest in energy among the three excited-state minima even in aqueous solution. Although the energy of $^1n\pi^*$ minimum is blue-shifted by solvation, its magnitude is very small, less than 0.1 eV. This is because the solute dipole moment in the out-of-plane direction increases the solute−solvent electrostatic interaction as mentioned above. The dipole moment in the gas phase is 1.74 D, while it largely increases to 4.63 D in aqueous solution, which is attributed to the polarization of NH bonds in the amino group induced by hydrogen bond formation with solvent H_2O molecules. In contrast to the $^1n\pi^*$ case, the ^1L_a state is stabilized by the solvation. The energy was red-shifted by 0.11 and 0.18 eV in CH_3CN and H_2O solutions, respectively. The dipole moment increases to 5.60 and 7.43 D in CH_3CN and H_2O, respectively, from the gas-phase value of 3.99 D. The energy change of ^1L_b state by the solvation is very small as seen in Table 2. This comes from the covalent nature of this state. The dipole moments in the gas phase, CH_3CN, and H_2O are 2.18, 2.82, and 3.04 D, respectively. The solvation energies at $(^1L_b)_{min}$, $(^1n\pi^*)_{min}$, and $(^1L_a)_{min}$ in aqueous solution were calculated to be 0.89, 1.00, and 1.03 eV, respectively.

Table 2 shows the vertical emission energies and oscillator strengths calculated at the excited-state energy minima. The oscillator strength is the largest for the ^1L_a state in both the gas phase and solutions. The ^1L_a emission energy in aqueous solution was calculated as 4.39 eV, which is red-shifted by 0.30 eV from the gas-phase value. Although the emission energy from the ^1L_b state is of similar value (4.41 eV) in H_2O, the oscillator strength is much smaller than that for ^1L_a. The emitting state in aqueous solution is discussed later.

In order to see the solvent effect on the solute electronic structures, we examined the microscopic solvation structures at the ground- and excited-state energy minima. The radial distribution functions (rdf's) for each state were obtained by solving the RISM equation under the solute partial charges corresponding to the target state. Figure 2 shows the rdf's between the N_1 and N_3 sites of solute adenine and the solvent sites. As seen in Figures 2a and 2b, the rdf's between the solute N sites and the CH_3 site of CH_3CN solvent have the first peaks at about 3.5 Å. These peaks become higher for $(^1L_a)_{min}$ than for $(gs)_{min}$ while lower for $(^1n\pi^*)_{min}$. The rdf's for $(^1L_b)_{min}$ are

(49) Voet, D.; Gratzer, W. B.; Cox, R. A.; Doty, P. *Biopolymers* **1963**, *1*, 193−208.

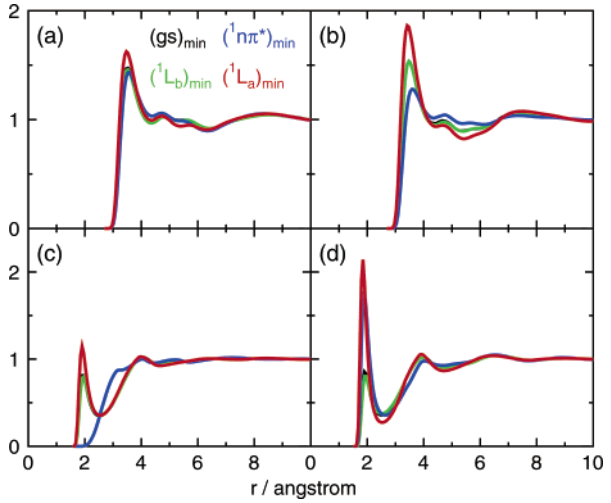

Figure 2. Radial distribution functions between solute and solvent sites for the ground- and excited-state minima. Black, red, green, and blue lines are for $(gs)_{min}$, $(^1L_a)_{min}$, $(^1L_b)_{min}$, and $(^1n\pi^*)_{min}$, respectively. (a) N_1-CH_3 in CH_3CN, (b) N_3-CH_3 in CH_3CN, (c) N_1-H in H_2O, and (d) N_3-H in H_2O.

very similar to those for $(gs)_{min}$. These trends are consistent with the energy shifts by solvation in CH_3CN shown in Table 2. The rdf's between the N_1 and N_3 sites of adenine and the H site of H_2O shown in Figure 2c and 2d have the first peaks at about 1.9 Å, which correspond to the hydrogen bonds between the N lone pairs of solute and the H atom of solvent. The peaks of $(gs)_{min}$ rdf's are of similar height at both of the N sites. The rdf's for $(^1L_b)_{min}$ are almost unchanged from those for $(gs)_{min}$ as in the case of CH_3CN. The peaks for $(^1L_a)_{min}$ become higher and the N_3-H rdf height is remarkably enhanced. These changes of the rdf's for $(^1L_b)_{min}$ and $(^1L_a)_{min}$ well correspond to the energy shifts shown in Table 2. For $(^1n\pi^*)_{min}$, the first peak of the N_1-H rdf disappears while that of the N_3-H rdf becomes higher, indicating that the hydrogen bond is broken around the N_1 site and becomes stronger around the N_3 site. Actually the partial charge at the N_1 site became slightly positive by the $^1n\pi^*$ excitation. Other many rdf's also show sharp peaks at about 2 Å corresponding to the hydrogen bonds: N_7-H, $H_{13}-O$, $H_{14}-O$, and $H_{15}-O$ in aqueous solution and $H_{13}-N$, $H_{14}-N$, and $H_{15}-N$ in acetonitrile. The hydrogen bond at the amino group is enhanced by the NH_2 out-of-plane deformation.

3.3. Conical Intersections. Conical intersection (CI) is an important ingredient to account for the ultrafast nonradiative decay of excited states. The CI between two electronic states with the same space and spin symmetry forms an $f-2$ dimensional surface with f being the number of degrees of freedom, and the lowest energy point on the CI surface is particularly important because it is regarded as a transition state point for nonadiabatic transition.

We first optimized the minimum energy geometries on the CIs of the ground state with the ^1L_a and $^1n\pi^*$ states, labeled as $(gs/^1L_a)_{CI}$ and $(gs/^1n\pi^*)_{CI}$, respectively, in H_2O and CH_3CN solvents as well as in the gas phase. The CASSCF optimized geometries were further corrected by eq 4. Although the MRMP energy difference at the CASSCF geometry was 0.6 eV for $(gs/^1L_a)_{CI}$, it was reduced to 0.2 eV by the correction. The largest change in the bond lengths due to the correction is 0.040 Å at the N_2C_3 bond in the gas phase. For $(gs/^1n\pi^*)_{CI}$, the energy gap correction was small and the gaps at both the corrected and uncorrected geometries were about 0.1 eV or less. Figure 3 shows the corrected geometries of these CI points in aqueous solution. The structures of $(gs/^1L_a)_{CI}$ and $(gs/^1n\pi^*)_{CI}$ are characterized by the out-of-plane deformation of the C_2 atom and the twisting around the N_1C_6 bond, respectively, as described in previous studies.[16,17,19,21−23] The change of these structural characteristics due to the solvation was small. The MRMP energies at the CI geometries are given in Table 3. The $(gs/^1n\pi^*)_{CI}$ energy is slightly lower than that of $(gs/^1L_a)_{CI}$ in both the gas phase and solutions. The CI energy at $(gs/^1n\pi^*)_{CI}$ in H_2O is higher by 0.1 eV than those in CH_3CN and the gas phase.

Table 3. Minimum Energies of CIs in the Gas Phase and Solution (in eV)

structure	symmetry	gas	CH_3CN	H_2O
$(gs/^1L_a)_{CI}$[a]	C_1	3.95/4.13	3.90/4.08	3.97/4.15
$(gs/^1n\pi^*)_{CI}$[a]	C_1	3.90/3.95	3.92/3.94	3.98/4.09
$(^1L_a/^1L_b)_{CI}$[a]	C_s	5.19/5.19	5.01/5.01	4.86/4.88
	C_1	4.94/5.09	4.87/4.97	4.82/4.93
$(^1L_a/^1n\pi^*)_{CI}$[a]	C_1	4.77/4.84	4.69/4.74	4.60/4.64
$(^1L_a/^1\pi\sigma^*)_{CI}$[b]	C_s	5.01/5.27	4.85/5.36	5.10/5.47
$(^1L_b/^1n\pi^*)_{CI}$[a]	C_s	4.59/4.66	4.63/4.70	4.76/4.82
	C_1	4.59/4.73	4.52/4.74	4.66/4.77

[a] Measured from the ground-state energy of $(gs)_{min}$ (C_1). [b] Estimated by energy difference from the ^1L_a state energy of $(^1L_a)_{min}$.

Since the ^1L_a state is the initially populated state by photoabsorption, the CIs of this state with other states are important to promote ultrafast nonradiative decay. We obtained the minimum energy points on the CIs with the ^1L_b, $^1n\pi^*$, and $^1\pi\sigma^*$ states, which are referred to as $(^1L_a/^1L_b)_{CI}$, $(^1L_a/^1n\pi^*)_{CI}$, and $(^1L_a/^1\pi\sigma^*)_{CI}$, respectively. The MRMP corrected geometries of these points in aqueous solution are shown in Figure 3. At $(^1L_a/^1L_b)_{CI}$ and $(^1L_a/^1n\pi^*)_{CI}$, the out-of-plane deformation of C_2 atom is observed as in the case of $(gs/^1L_a)_{CI}$. We found that the solvation decreases the dihedral angle $\delta(C_6N_1C_2N_3)$ at $(^1L_a/^1L_b)_{CI}$ and increases it at $(^1L_a/^1n\pi^*)_{CI}$. The bond lengths at these CIs are also affected by the solvation. A notable change is the N_7C_8 distance at $(^1L_a/^1L_b)_{CI}$, which stretches by 0.03 Å by the aqueous solvation. In contrast to the CIs with the ground state, the energies of $(^1L_a/^1L_b)_{CI}$ and $(^1L_a/^1n\pi^*)_{CI}$ are lowered by the solvation as seen in Table 3. At $(^1L_a/^1L_b)_{CI}$, the CI energy becomes lower by 0.10 and 0.14 eV in CH_3CN and H_2O solvents, respectively, than the gas-phase one. A large solvent effect on the energy lowering is also obtained for $(^1L_a/^1n\pi^*)_{CI}$ in aqueous solution, 0.19 eV. Note that we took the average energy of two states as the energy at CI. The N_9H_{13} distance at $(^1L_a/^1\pi\sigma^*)_{CI}$ in the gas phase becomes longer by 0.015 Å than that at $(gs)_{min}$, though such a change in N_9H_{13} distance is reduced by the solvation. The solvent effect on the CI geometry was mainly observed at the bond distances in aromatic rings. As seen in Table 3, the CI energy is located as 5.14, 5.11, and 5.28 eV in the gas phase, CH_3CN and H_2O solvents, respectively.

We further optimized the CI between the ^1L_b and $^1n\pi^*$ states, $(^1L_b/^1n\pi^*)_{CI}$. As seen in Figure 3, the CI geometry is characterized by the out-of-plane bend of the C_6N_{10} bond. The energy at $(^1L_b/^1n\pi^*)_{CI}$ is not so affected by the solvation because both of the electronic states are of a covalent type. The energy increases only by 0.06 eV in aqueous solution.

We now examine the solvent effect on the geometries and energies of CIs. The CI between two electronic states is

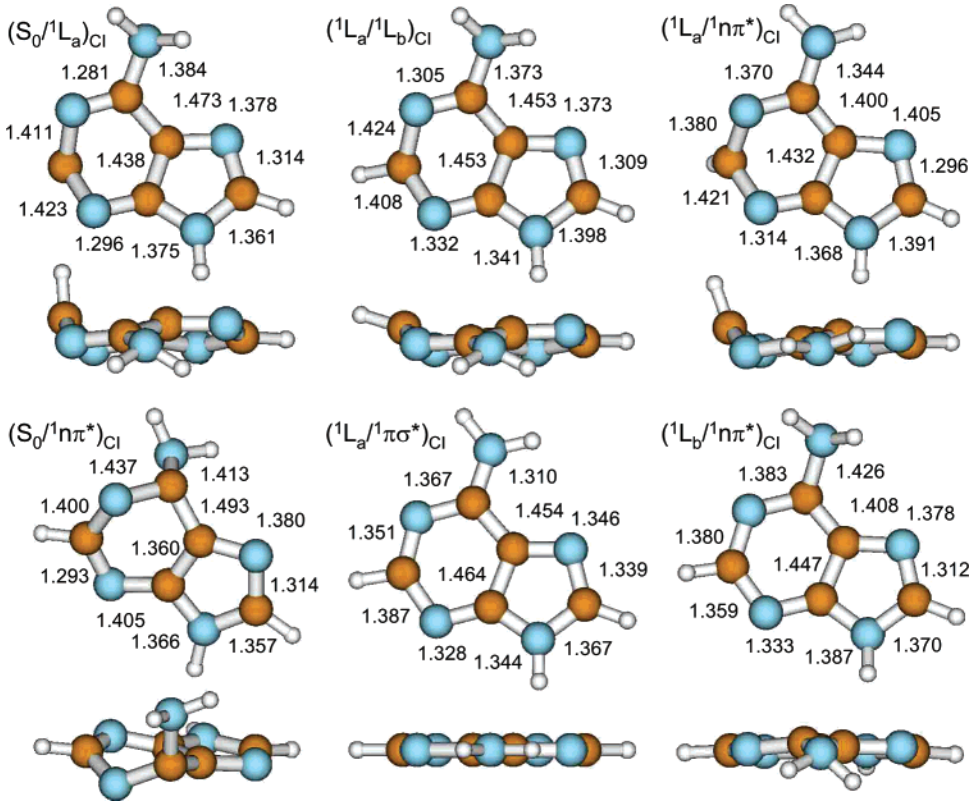

Figure 3. Optimized geometries of minimum energy CIs in aqueous solution. Bond lengths are in angstroms. For colors for atoms, see Figure 1.

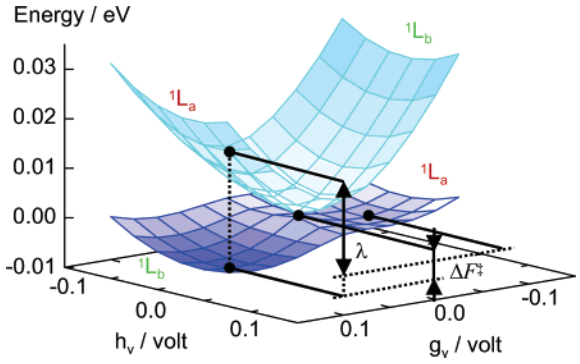

Figure 4. Free energy surface at $(^1L_a/^1L_b)_{CI}$ geometry in aqueous solution as a function of displacement along $\mathbf{g}_V^{IJ}$ and $\mathbf{h}_V^{IJ}$. Definitions of activation ($\Delta F^\ddagger$) and reorganization (λ) energies are also shown.

characterized by two coordinates, one is the tuning coordinate $\mathbf{g}^{IJ}$ given by the difference between gradient vectors for the states I and J and the other is the coupling coordinate $\mathbf{h}^{IJ}$ given by the nonadiabatic coupling elements between the two states.[50] Although the vectors $\mathbf{g}^{IJ}$ and $\mathbf{h}^{IJ}$ depend only on the nuclear coordinates in the gas phase, they have the components of solvation coordinates in addition to the solute nuclear ones in solution. Thus these two vectors are expressed as $\mathbf{g}^{IJ} = \mathbf{g}_R^{IJ} + \mathbf{g}_V^{IJ}$ and $\mathbf{h}^{IJ} = \mathbf{h}_R^{IJ} + \mathbf{h}_V^{IJ}$, where the solute components $\mathbf{g}_R^{IJ}$ and $\mathbf{h}_R^{IJ}$ have $3 \times 15 = 45$ nonzero elements, while the solvent components $\mathbf{g}_V^{IJ}$ and $\mathbf{h}_V^{IJ}$ have 15 elements corresponding to the electrostatic potentials acting on the solute atomic sites. Note that the LJ potentials do not contribute to these vectors in the present model.[34] The magnitudes of these vectors were obtained at the CI geometries. For example, in aqueous solution, those of tuning vectors are $|\mathbf{g}_R^{IJ}| = 0.25$ and $|\mathbf{g}_V^{IJ}| = 0.31$ at $(gs/^1L_a)_{CI}$ in atomic unit and $|\mathbf{g}_R^{IJ}| = 0.20$ and $|\mathbf{g}_V^{IJ}| = 0.23$ at $(^1L_a/^1L_b)_{CI}$, respectively. The coupling vectors are $|\mathbf{h}_R^{IJ}| = 9.6 \times 10^{-2}$ and $|\mathbf{h}_V^{IJ}| = 8.3 \times 10^{-3}$ at $(gs/^1L_a)_{CI}$ and $|\mathbf{h}_R^{IJ}| = 9.3 \times 10^{-2}$ and $|\mathbf{h}_V^{IJ}| = 2.6 \times 10^{-3}$ at $(^1L_a/^1L_b)_{CI}$. Although we cannot compare $|\mathbf{g}_R^{IJ}|$ and $|\mathbf{g}_V^{IJ}|$ directly because their dimensions are different, it can be easily observed that the solvent contribution to the tuning coordinate is much larger than the coupling one. The same was true at other CI points in H_2O and all CIs in CH_3CN solvent. We can therefore conclude that the solvent polarization mainly participates in determining the CI by matching the energies of two states.

At the CI geometry, the solvent polarization is not equilibrium to the solute charge distribution in both of the electronic states as in the case of electron-transfer reactions. Figure 4 shows the free energy surface near the CI point $(^1L_a/^1L_b)_{CI}$ in aqueous solution as a function of the displacement coordinates along the vectors $\mathbf{g}_V^{IJ}$ and $\mathbf{h}_V^{IJ}$, where we can find the CI point at the origin and two free energy minima corresponding to the ^1L_a and ^1L_b states. Note that the solute nuclear coordinates are fixed to those at the CI geometry. We calculated the free energy of solvent polarization required to reach the CI point from the free energy minimum of each electronic state, i.e., the activation energy, by

$$\Delta F_I^\ddagger = F_{LR}^I(\mathbf{V}_{CI},\mathbf{U}_{CI}) - F_{LR}^I(\bar{\mathbf{V}}_I,\bar{\mathbf{U}}_I) \qquad (5)$$

where $\mathbf{V}_{CI}$ and $\mathbf{U}_{CI}$ are the solvent potentials at CI. The equilibrium potentials $\bar{\mathbf{V}}_I$ and $\bar{\mathbf{U}}_I$ were obtained by the LRFE optimization with respect to $\mathbf{V}$ and $\mathbf{U}$. We also estimated the

(50) Yarkony, D. R. *J. Phys. Chem. A* **2001**, *105*, 6277−6293.

reorganization energy λ. For the state I, it is calculated by

$$\lambda_I = F^I_{\mathrm{LR}}(\bar{\mathbf{V}}_J,\bar{\mathbf{U}}_J) - F^I_{\mathrm{LR}}(\bar{\mathbf{V}}_I,\bar{\mathbf{U}}_I) \qquad (6)$$

That for the state J, λ_J, is also evaluated similarly.

Table 4 summarizes the calculated $\Delta F^{\ddagger}$ and λ. For $(\mathrm{gs}/^1\mathrm{n}\pi^*)_{\mathrm{CI}}$, only $\Delta F^{\ddagger}$ for the ground state was obtained because the $^1\mathrm{n}\pi^*$ surface was so flat that the minimum point was not detected by the optimization. These energies at $(^1\mathrm{L}_a/^1\pi\sigma^*)_{\mathrm{CI}}$ were estimated with solute charges fixed because the optimization led to other states when the electronic structures were explicitly calculated. The results in Table 4 indicate that the nonequilibrium solvation effect is large at $(^1\mathrm{L}_a/^1\pi\sigma^*)_{\mathrm{CI}}$ in aqueous solution, where $\Delta F^{\ddagger}$ for the $^1\pi\sigma^*$ state was calculated to be 0.49 eV. The reorganization energy at this CI is also large, 0.51 eV, which is of similar value to those at $(^1\mathrm{L}_a/^1\mathrm{n}\pi^*)_{\mathrm{CI}}$, 0.62 and 0.51 eV, respectively. It should be noticed that the results for $(^1\mathrm{L}_a/^1\pi\sigma^*)_{\mathrm{CI}}$ do not include the contribution of solute electronic polarization, whereas those for $(^1\mathrm{L}_a/^1\mathrm{n}\pi^*)_{\mathrm{CI}}$ include it. The $^1\pi\sigma^*$ state is expected to be further stabilized if the solute is polarized. Such stabilization was observed when the solute geometry as well as solvent potentials were optimized with respect to the $^1\pi\sigma^*$ state. The minimum energy was calculated to be 5.11 eV in the gas phase, and it was largely lowered by 0.42 and 1.46 eV in CH_3CN and H_2O solutions, respectively, which is consistent with the results of Ritze et al.[5] Note that, although the $^1\pi\sigma^*$ state was higher in energy than the $^1\mathrm{L}_a$ and $^1\mathrm{L}_b$ ones in the gas phase, it became lower than those in the solvents.

3.4. Solvent Effects on the Radiationless Decay Mechanism. The absorption spectrum observed at the region around 260 nm in aqueous solution[49] is attributed to the transition to the $^1\mathrm{L}_a$ state because of its exceedingly larger oscillator strength than the $^1\mathrm{L}_b$,$^1\mathrm{n}\pi^*$, and $^1\pi\sigma^*$ states. Since the inversion barrier of the amino group for the ground state is considerably low even in aqueous solution, the amino inversion occurs easily and the transition near the planar geometry may become important. The vertical excitation energy calculated at the optimized geometry, 4.88 eV, agrees well with the experiment.

The fluorescence spectrum has the peak at 320 nm.[51,52] Although the $^1\mathrm{L}_a$ state has a very large oscillator strength with the ground state, the potential energy surface of this state is unstable with respect to the out-of-plane deformation mode with the imaginary frequency and the optimized planar geometry corresponds to the saddle point. The $^1\mathrm{L}_b$ state surface, on the other hand, has the minimum at the planar geometry. In Figure 5, we show the calculated energy levels of $^1\mathrm{L}_a$, $^1\mathrm{L}_b$,$^1\mathrm{n}\pi^*$, and $^1\pi\sigma^*$ states at some important geometries in the gas phase and aqueous solution. We took the solvent potentials **V** and **U** obtained for the labeled state for calculating the energy levels in each column. The $^1\mathrm{L}_a$ state energy at the $(^1\mathrm{L}_b)_{\mathrm{min}}$ geometry is slightly lower than that at $(^1\mathrm{L}_a)_{\mathrm{min}}$ in both the gas phase and aqueous solution. This is because the dynamic electron correlation energy is larger at $(^1\mathrm{L}_b)_{\mathrm{min}}$ than that at $(^1\mathrm{L}_a)_{\mathrm{min}}$, indicating the energy minimum of this state is rather close to the $(^1\mathrm{L}_b)_{\mathrm{min}}$ geometry than the $(^1\mathrm{L}_a)_{\mathrm{min}}$ one at the MRMP level. In aqueous solution, the energy difference between the $^1\mathrm{L}_a$ and $^1\mathrm{L}_b$ states is very small at the planar geometries, less than 0.2 eV, and the $(^1\mathrm{L}_a/^1\mathrm{L}_b)_{\mathrm{CI}}$ energy is closely located to these energies, indicating

Table 4. Activation and Reorganization Energies ($\Delta F^{\ddagger}$ and λ, Respectively) of CIs in Solution Calculated at CASSCF Level (in eV)

	$\Delta F^{\ddagger}$		λ	
structure	CH_3CN	H_2O	CH_3CN	H_2O
$(\mathrm{gs}/^1\mathrm{L}_a)_{\mathrm{CI}}$	0.03/0.02	0.10/0.05	0.10/0.10	0.29/0.29
$(\mathrm{gs}/^1\mathrm{n}\pi^*)_{\mathrm{CI}}$	0.02/—[a]	0.06/—[a]	—[a]	—[a]
$(^1\mathrm{L}_a/^1\mathrm{L}_b)_{\mathrm{CI}}$	0.01/0.01	0.03/0.05	0.03/0.03	0.15/0.16
$(^1\mathrm{L}_a/^1\mathrm{n}\pi^*)_{\mathrm{CI}}$	0.02/0.02	0.15/0.14	0.09/0.08	0.62/0.51
$(^1\mathrm{L}_a/^1\pi\sigma^*)_{\mathrm{CI}}$[b]	0.00/0.08	0.00/0.49	0.08/0.08	0.51/0.51
$(^1\mathrm{L}_b/^1\mathrm{n}\pi^*)_{\mathrm{CI}}$	0.01/0.01	0.01/0.06	0.04/0.04	0.14/0.13

[a] See text. [b] Estimated with solute charges fixed to those at CI.

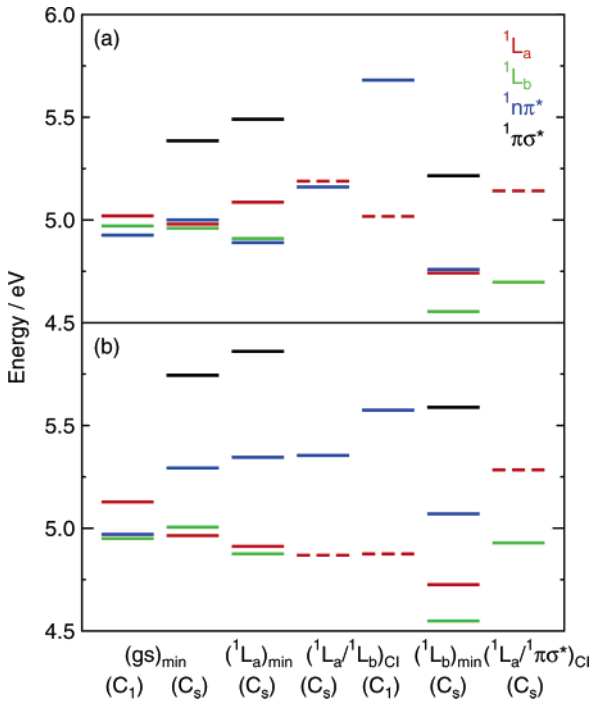

Figure 5. Energy levels of excited states at some important energy minima and CIs. Red, green, blue, and black lines are for $^1\mathrm{L}_a$, $^1\mathrm{L}_b$, $^1\mathrm{n}\pi^*$, and $^1\pi\sigma^*$ energies, respectively. Dashed line is the energy of CI. (a) Gas phase and (b) aqueous solution.

these two states are vibronically coupled. To examine the extent of such vibronic coupling, we further obtained the $(^1\mathrm{L}_a/^1\mathrm{L}_b)_{\mathrm{CI}}$ geometry assuming C_s symmetry. The results are included in Table 3 and Figure 5. Although the planar $(^1\mathrm{L}_a/^1\mathrm{L}_b)_{\mathrm{CI}}$ energy is about 0.2 eV higher than that of the minimum energy CI point in the gas phase, it is almost the same as that of the nonplanar CI in aqueous solution, which means that the low-energy CI between the $^1\mathrm{L}_a$ and $^1\mathrm{L}_b$ states occurs at a wide area of the geometry space. Considering these results, we can assert that the emitting state in aqueous solution is a vibronically coupled state between the $^1\mathrm{L}_a$ and $^1\mathrm{L}_b$ states and the intensity is borrowed from the $^1\mathrm{L}_a$ state. In the gas phase, the $(^1\mathrm{L}_a/^1\mathrm{L}_b)_{\mathrm{CI}}$ energy becomes higher, and thus the vibronic coupling is weaker than that in H_2O. In CH_3CN solvent, its magnitude is an intermediate between the gas phase and aqueous solution.

For 9H-adenine, mainly three types of decay routes of the $^1\mathrm{L}_a$ state were proposed in previous theoretical studies; (i) the direct decay channel from the $^1\mathrm{L}_a$ state to $(\mathrm{gs}/^1\mathrm{L}_a)_{\mathrm{CI}}$, (ii) the decay path through the $^1\mathrm{n}\pi^*$ state to $(\mathrm{gs}/^1\mathrm{L}_a)_{\mathrm{CI}}$ or $(\mathrm{gs}/^1\mathrm{n}\pi^*)_{\mathrm{CI}}$, and (iii) the pathway via the $^1\pi\sigma^*$ state.

(51) Callis, P. R. *Ann. Rev. Phys. Chem.* **1983**, *34*, 329−357.
(52) Daniels, M.; Hauswirth, W. *Science* **1971**, *171*, 675−677.

Route (i) is the diabatic decay path of the ^1L_a state with the ring puckering deformation. In aqueous solution, the ^1L_a state energy is red-shifted, and therefore the initial fluorescence state is considered to be a vibronically coupled state between ^1L_a and ^1L_b as mentioned above. This $^1L_a-^1L_b$ vibronically coupled state can directly decay to the ground state through $(gs/^1L_a)_{CI}$, and thus route (i) becomes more accessible in aqueous solution than in the gas phase.

Route (ii), the pathway including the nonadiabatic transition from the ^1L_a to $^1n\pi^*$ state, becomes difficult to access in polar solvent in contrast to the case of route (i). As seen in Figure 5, the $^1n\pi^*$ state energy in the gas phase is below or very close to the ^1L_a one at all the planar geometries. Thus a strong coupling between the initially populated ^1L_a state and $^1n\pi^*$ one is expected. However, in aqueous solution, the $^1n\pi^*$ state is blue-shifted and the energy is higher than ^1L_a by 0.3−0.5 eV except at the nonplanar equilibrium geometry of the ground state. We can therefore expect that the nonadiabatic transition from ^1L_a to $^1n\pi^*$ near the planar geometry is largely suppressed in aqueous solution, while such a process is easily to occur in the gas phase. The same situation as that in H_2O is obtained for CH_3CN solution, though the degree of $^1n\pi^*$ blue shift is smaller.

Route (iii), the NH dissociative channel via the $^1\pi\sigma^*$ state, is considered to participate in the decay process. In the gas phase, the $^1\pi\sigma^*$ state energy at $(gs)_{min}$ is considerably higher than the ^1L_a one. This is also true at $(^1L_a)_{min}$ and $(^1L_b)_{min}$, as shown in Figure 5. Nevertheless, the energy of $(^1L_a/^1\pi\sigma^*)_{CI}$, which is regarded as a bottleneck for the nonadiabatic transition from the ^1L_a to $^1\pi\sigma^*$ state, is only 0.06 eV higher than that of $(^1L_a)_{min}$ and of very similar value to that of $(^1L_a/^1L_b)_{CI}$ at the planar structure. Thus the decay process via route (iii) would easily occur in the gas phase. In aqueous solution, the barrier height of the transition, i.e., the energy difference between $(^1L_a)_{min}$ and $(^1L_a/^1\pi\sigma^*)_{CI}$, is raised to 0.37 eV due to the stabilization of $(^1L_a)_{min}$ and the destabilization of $^1\pi\sigma^*$ state as seen in Figure 5. The contribution of the $^1\pi\sigma^*$ channel becomes less important in aqueous solution.

A decay route involving the ^1L_b state has been also discussed.[17,21−23] We found that the ^1L_a state is very close in energy to the ^1L_b one even at the equilibrium geometry of ^1L_b in aqueous solution, as shown in Figure 5. This suggests that the ^1L_b state is vibronically coupled with ^1L_a and thus the direct path passing through $(gs/^1L_a)_{CI}$ is considered to be responsible for the decay of this state. It is also noted the minimum energy $(^1L_b/^1n\pi^*)_{CI}$ is located at 0.17 eV above the ^1L_b state minimum and therefore the formation of $^1n\pi^*$ state may be possible even in aqueous solution.

Two different lifetimes of the excited-state are observed in gas phase by the experiments. The fast component of 0.1 ps has been assigned to route (i) and/or (iii) because these pathways have no or very low-energy barrier, which is consistent with the present results. Route (iii) may become important in the gas phase with increasing excitation energy because the energy barrier for the transition to $^1\pi\sigma^*$ state is very small as described above. On the other hand, the slow decay of 1 ps has been attributed to route (ii). In this case, there are two possible pathways to reach the ground state, one is through $(gs/^1L_a)_{CI}$ and the other is through $(gs/^1n\pi^*)_{CI}$. For the former pathway, the transition state exists near the $(^1L_a/^1n\pi^*)_{CI}$ point whose energy was calculated to be 0.6 eV above the $^1n\pi^*$ state energy minimum (see Tables 2 and 3). Note that Blancafort[22] estimated the barrier heights of 0.17 eV. As the barrier height for the latter pathway, two much different values are reported, 0.60 and 0.08 eV.[22,23] Although the nonadiabatic transition to the $^1n\pi^*$ state near the planar geometry can be a slow decay path in the gas phase, it is not likely to occur in the aqueous solution because such a transition is largely suppressed by the shifts of ^1L_a and $^1n\pi^*$ energies by the solvation. This is consistent with the experimental observation that the fluorescence decays very rapidly in a monoexponential manner.

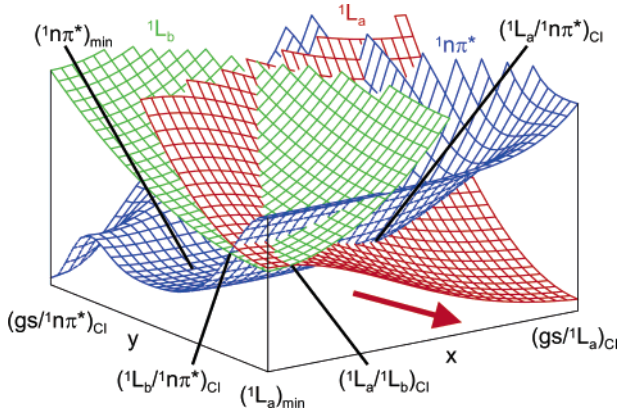

Figure 6. Scheme of radiationless decay mechanism of 9H-adenine in aqueous solution. Coordinates *x* and *y* roughly correspond to the displacements to $(gs/^1L_a)_{CI}$ and $(gs/^1n\pi^*)_{CI}$, respectively. ^1L_a, ^1L_b, and $^1n\pi^*$ surfaces are represented by red, green, and blue colors.

The energy dependence of the excited-state lifetime has been examined by experiments. This dependence may be attributed to two mechanisms. First, in route (i), the excited-state lifetime is determined by the mixing weight of the ^1L_a state wave function to that of the ^1L_b state at the $^1L_a-^1L_b$ vibronic coupling region. The change of lifetime is consistent with the present result because the weight of the ^1L_a state increases with increasing energy. Since the vibronic coupling is weaker in CH_3CN than in H_2O, the lifetime in CH_3CN solvent is expected to be longer than that in aqueous solution. Second, route (iii) may open at a larger excitation energy even in aqueous solution.[11] As described above, the energy of $(^1L_a/^1\pi\sigma^*)_{CI}$ is 0.06 and 0.37 eV higher than that of $(^1L_a)_{min}$ in the gas phase and aqueous solution, respectively.

To summarize the present results, we depicted a scheme of radiationless decay of 9H-adenine in aqueous solution in Figure 6. As discussed above, two solvation effects should be noted. First, the ^1L_a state is red-shifted and becomes close in energy to the ^1L_b one at the region around $(^1L_a)_{min}$ and $(^1L_b)_{min}$. This enhances the vibronic coupling between these states and thus the direct decay to the $(gs/^1L_a)_{CI}$, i.e., the decay through route (i), becomes most likely to occur. Second, the $^1n\pi^*$ state is blue-shifted, and thus the nonadiabatic transition to this state, i.e., the decay through route (ii), becomes difficult to take place. In Figure 6, the ^1L_a state surface intersects the $^1n\pi^*$ one at nonplanar geometry, but the nonadiabatic transition from ^1L_a to $^1n\pi^*$ is not likely to occur at this region because the amplitude of the wave packet propagating on the ^1L_a surface is considered to be small at this region which is far from the minimum energy ring puckering path.

It is also noted that the solvent fluctuation affects the nonadiabatic transition dynamics around the CI.[53,54] When considering that the solvent reorganization energy of 0.15 eV at $(^1L_a/^1L_b)_{CI}$ is comparable to the energy gap between the two states, the solvent fluctuation dynamics may play an important role in forming the vibronically coupled states between ^1L_a and ^1L_b.

4. Conclusions

We studied the excited-state electronic structures of 9H-adenine in aqueous and acetonitrile solutions to explore the solvent effects on the radiationless decay mechanism. The equilibrium geometries of the ground and excited (^1L_a, ^1L_b,$^1n\pi^*$, and $^1\pi\sigma^*$) states and the conical intersections among these states were obtained by the LRFE method. The LRFE was calculated by the RISM-SA-CASSCF method, and the dynamic electron correlation was incorporated by the MRMP method.

We addressed the question why the excited-state decay signal of 9H-adenine is monoexponential with the subpicosecond lifetime in a polar solvent, while it is biexponential with the subpicosecond and picosecond lifetimes in the gas phase. Since the ^1L_a state is red-shifted and becomes close in energy to the ^1L_b one, the vibronic coupling between these states is largely enhanced in aqueous solution. Actually the conical intersection occurs in a wide area of the geometry space in solution. Thus the direct decay of this vibronically coupled state to the ground state through the $(gs/^1L_a)_{CI}$ point is considered to be the dominant decay pathway in the solution. The $^1n\pi^*$ state is proposed to participate in the radiationless decay in the gas phase, the longer time component. Although the energy gap between the $^1n\pi^*$ and ^1L_a states is small in the gas phase, it becomes large in aqueous solution because the $^1n\pi^*$ state is blue-shifted while the ^1L_a one is red-shifted. Thus the decay pathway through the $^1n\pi^*$ state is suppressed in solution. This may be the reason why the slow decay component is not observed in aqueous solution. The decay path via the $^1\pi\sigma^*$ state was also examined. Although the barrier height for the transition from the ^1L_a to $^1\pi\sigma^*$ state was very low in the gas phase, it was raised by the aqueous solvation.

The present study provided some new insights to the radiationless decay mechanism of 9H-adenine in polar solvents. However, the present results are still qualitative because we optimized the geometries of free energy minima and conical intersections at the CASSCF level, while their energies were calculated at the MRMP level. Since the dynamic electron correlation effect is particularly important for the ^1L_a state, it will be desirable to employ more accurate wave functions such as a multireference configuration interaction method to obtain more quantitative results.

We focused only on the free energy characteristics of excited-state 9H-adenine in solution. To fully understanding the radiationless decay mechanism, the dynamics calculations will be required. We adopted the electrostatic and LJ potentials as the solvation coordinates representing the collective motion of solvent. Since these variables are regarded as stochastic ones, the nonadiabatic transition dynamics around the conical intersections can be described by stochastic equations of motion such as a generalized Langevin equation. Such a problem is the subject of future work.

Acknowledgment. This work was supported by the Grant-in-Aid for Scientific Research from the Ministry of Education and Science in Japan.

Supporting Information Available: Complete ref 46. Actives spaces and state averaging used for the optimizations (Table SI1), Cartesian coordinates of energy minima and conical intersections in the gas phase, acetonitrile, and aqueous solution (Tables SI2 and SI3), and structures of energy minima in aqueous solution (Figure SI1). This material is available free of charge via the Internet at http://pubs.acs.org.

JA0669169

(53) Kühl, A.; Domcke, W. *J. Chem. Phys.* **2002**, *116*, 263−274.
(54) Cederbaum, L. S.; Gindensperger, E.; Burghardt, I. *Phys. Rev. Lett.* **2005**, *94*, 113003.